Open Access

Catalysis Research

LIDSEN Publishing Inc.

Original Research

Acetonitrile Combustion over Copper-Based Nanocatalysts: A Structure-Performance Relationship Study

Jéssica A. P. Ponciano, Marcelo S. Batista *

Federal University of São João del Rei, Campus Alto Paraopeba, highway MG 443, Km 5, Ouro Branco–MG 36420-000, Brazil; E-Mails: jessica.ponciano20@hotmail.com; marcelobatista@ufsj.edu.br

* **Correspondence:** Marcelo S. Batista; E-Mail: marcelobatista@ufsj.edu.br

Academic Editor: Md Ariful Ahsan

Special Issue: Applications of Environmental Catalysis

Catalysis Research
2022, volume 2, issue 1
doi:10.21926/cr.2201002

Received: December 01, 2021
Accepted: January 20, 2022
Published: January 26, 2022

Abstract

In this paper, the relationship between activity and structure of Cu^{2+} in different chemical environments of Cu-BETA, La_2CuO_4, and CuO nanocatalysts was systematically investigated for acetonitrile combustion. The study revealed that exchanged and octahedral species of Cu^{2+} coexist in Cu-BETA, while octahedral species are dominant in CuO and La_2CuO_4. All nanocatalysts achieved high conversion rates of acetonitrile, which rapidly increased with temperature. CuO and La_2CuO_4 led to the formation of undesired products such as N_2O and NO. On the other hand, Cu-BETA showed high acetonitrile conversion along with a high N_2 yield. The excellent performance of Cu-BETA can be attributed to the easy reducibility of the highly dispersed Cu-species and the small crystallite size. Cu-BETA also exhibited exceptional stability. Therefore, the high conversion rate and the high N_2 yield make Cu-BETA a promising catalyst for acetonitrile combustion.

Keywords

Catalytic combustion; acetonitrile; copper; perovskite; BETA zeolite

1. Introduction

Acetonitrile (CH_3CN) is widely used as an industrial solvent, but it also finds applications in the production of acrylic plastic, acrylic fibers, resins, nitrile elastomers, and appears in numerous hazardous waste streams. Acetonitrile found in industrial exhaust gases is dangerous to humans and the environment; therefore, its abatement is extremely important [1-3]. Treatment of acetonitrile by traditional thermal combustion technique is controlled by chain-terminating reaction sequences at elevated temperatures (above 1000 °C) and often leads to the formation of undesirably large amounts of nitrogen oxides and HCN [4]. According to earlier studies [3, 5-7], the selective catalytic combustion (SCC) of acetonitrile toward N_2 and CO_2 is the most efficient and environmentally benign route, owing to its high purification efficiency, low operation cost at lower temperatures, and fewer secondary pollutants.

Zhang's group [8, 9] studied the combustion of acrylonitrile and acetonitrile over various metals (M = Cu, Co, Fe, V, Mn, Pd, Ag, Pt), and reported good performance of copper-modified mesoporous material. Cu/SBA-15 exhibited a nearly complete conversion of acetonitrile and acrylonitrile together with achieving a good N_2 selectivity of 80% (>350 °C) and 64% (>400 °C), respectively. Nanba et al. [10] studied the SCC using catalysts of various metals (Mg, Ca, Mn, Fe, Co, Ni, Cu, Zn, Ga, Pd, Ag, and Pt) supported on several frameworks (Al_2O_3, SiO_2, TiO_2, ZrO_2, MgO and ZSM-5). Among them, Cu-ZSM-5 achieved full conversion at above 350 °C associated with ~80% N_2 selectivity. Although copper is considered an interesting transition metal for SCC, its conversion and N_2 selectivity depend very much on the catalyst structure.

La_2CuO_4 is a perovskite-like type mixed oxide and is an interesting catalyst in terms of its reactivity; it has versatility in both oxidation and reduction reactions. It has been demonstrated that NO-SCR and acrylonitrile-SCC performance, along with N_2 selectivity, is improved by the incorporation of Cu^{2+} into the lattice of perovskites [11, 12]. The best performance was attributed to the redox properties inherent in the perovskite-type oxides. These features of perovskite-type materials inspired us to believe that these materials, especially using Cu^{2+}, could offer promising performances in acetonitrile catalytic combustion.

The literature reports some studies discussing the performance of catalysts prepared via impregnation for the acrylonitrile-SCC [3, 13, 14] and rare works related to acetonitrile-SCC [7, 8]. In terms of the zeolite topology, BETA was the most effective material among various commercial zeolites (MFI, FER, MOR, FAU) with similar Si/Al ratios for the decomposition of N_2O [15] and exhibited superior activity in comparison with ZSM-5 [16]. Recently, the influence of different active center structures over Cu-BETA was investigated for HCN-SCC [17]. DFT simulation results revealed that the geometry of the active centers greatly influences the final activity, selectivity, and even reaction mechanism. Therefore, in this study, to the best of our knowledge, a relationship was established between the activity and structure of Cu^{2+} in a different chemical environment using Cu-BETA, La_2CuO_4, and CuO catalysts, which were systematically investigated for acetonitrile-SCC. Various characterizations, including X-ray fluorescence (XRF), X-ray diffraction (XRD), temperature-programmed reduction by hydrogen (H_2-TPR), and UV-VIS spectroscopy, were employed.

2. Materials and Methods

2.1 Catalyst Preparation

The Cu-BETA catalyst was prepared by three consecutive ion-exchange reactions employing a commercial NH_4-BETA zeolite (BETA Products Standard from Tricat, SiO_2/Al_2O_3 molar ratio of 24.5) and an aqueous solution of cupric nitrate at room temperature for 12 h. After each step, the solid was filtered, washed with distilled water, and dried at 110 °C. Finally, the Cu-BETA catalyst was obtained after final calcination at 650 °C for 2 h. CuO catalyst was prepared by calcination of cupric nitrate at 650 °C for 2 h at the rate of 10 °C/min.

La_2CuO_4 catalyst was prepared by the polymerization method (also known as Citrate or Pechini). Copper and lanthanum nitrates were used as the initial reactants for the synthesis of perovskite-type oxide. These nitrates contain cations in stoichiometric quantity. They were dissolved in water, followed by the addition of citric acid and ethylene glycol in equimolar amounts. The mixture was stirred and the excess water was evaporated at 80 °C. A resin-like material was formed after being dried at 110 °C for overnight. The material was deagglomerated and calcined at 550 °C for 3 h and 800 °C for 5 h (heating rate 5 °C/min) in static air.

2.2 Catalyst Characterization

The catalysts were characterized using a couple of techniques, including X-ray fluorescence (XRF), X-ray diffractometry (XRD), temperature-programmed reduction by hydrogen (H_2-TPR), and UV-VIS spectroscopy. XRF analyses were carried out in the equipment Shimadzu EDX 720/800HS with 200 mg of catalyst and a flow of 200 mL/min of He. XRD analyses were performed by adopting the powder method using a Rigaku diffractometer (Miniflex 600) with Cu tube, Ni-filtered, operating at 40 kV, 15 mA, and employing CuKα radiation. The speed of the goniometer was 2°(2θ)/min; the 2θ angle ranges between 5 and 80°. The average particle size was calculated using the half-width at half-height of the most intense peak of CuO (2θ = 38.7°) and the Debye-Scherrer equation ($\mathrm{D_{hkl}} = \mathrm{k\lambda/\beta cos(\theta)}$).

H_2-TPR analyses were performed on SAMP3 apparatus (Termolab Equipment, Brazil) equipped with a thermal conductivity detector (TCD). A trap was used to remove the water stemming due to reduction before the gas of the reactor outlet was sent to the TCD. TPR started with a ramp of 10 °C/min from 50 to 1000 °C. A flow rate of 30 mL/min from a high purity mixture of 2 vol.% H_2 in Ar and 100 mg of Cu-BETA, 50 mg La_2CuO_4, and 10 mg CuO were used.

The diffuse reflectance spectra were recorded employing a UV–VIS spectrophotometer (Shimadzu UV 2700). $BaSO_4$ was used as the reference material. Before the measurement, the samples were dried at 120 °C for 2 h to remove any water molecules or OH groups. Samples were scanned in the range of 200–800 nm. The reflectance data were converted in terms of the Schuster-Kubella-Munk function, $F(R) = (1-R)^2/2R$, where R represents the diffuse reflectance obtained directly from the spectrometer.

2.3 Catalytic Evaluation

The catalysts were evaluated in the selective combustion reaction of acetonitrile (CH_3CN-SCC) using a quartz wool bed "U" reactor. The sample contained 8.6 mg of copper fed with a continuous

flow of 40 mL/min of a mixture containing 2.8 vol.% CH_3CN in synthetic air. The reactor operated at atmospheric pressure, and the reaction temperature varied from 100 to 600 °C. The reactor was coupled in line with a mass spectrometer (THERMO) for gas analysis: N_2 (m/z = 28), O_2 (m/z = 32 and 16), NO + N_2O (m/z = 30), NH_3 (m/z = 17), HCN (m/z = 27), NO_2 (m/z = 46), CH_3CN (m/z = 41) and CO_2 (m/z = 44). Conversion of CH_3CN was calculated using Equation 1. The turnover frequency (TOF) was calculated in terms of the mole of reagent consumed per unit time and mole of copper.

$$\text{Conversion } (\%) = \left(\frac{CH_3CN_{(in)} - CH_3CN_{(out)}}{CH_3CN_{(in)}}\right) \times 100 \quad (1)$$

3. Results and Discussion

Crystalline phases obtained after synthesis were identified by XRD analysis. Figure 1 depicts the diffractogram of Cu-BETA, CuO, and La_2CuO_4 catalysts. The diffractogram of CuO catalyst exhibited the characteristic peaks of copper oxide (PDF#41–0254). Cu-BETA presented diffraction peaks corresponding to zeolite BETA (PDF#48–0074). In addition, Cu-BETA also showed peaks corresponding to CuO (2θ= 35.5, 38.7, and 48.7°), indicating that copper species underwent precipitation during the ion exchange reaction. La_2CuO_4 showed reflection lines for orthorhombic perovskite structure (PDF#70–0449) and also for CuO, suggesting that the copper oxide was formed together with La_2CuO_4. The relative amount of perovskite (87%) and copper oxide (13%) phases present in the samples was determined using the integrated intensity of the most intense peak of the corresponding phases [18, 19]. No evidence of La_2O_3 peaks (PDF#02–0688) or Cu_2O peaks (PDF#35–1091) could be gathered by XRD. These results are in good agreement with the literature data [12, 18], suggesting that after calcination, a small amount of CuO is observed along with the La_2CuO_4 phase. However, the existence of tiny La_2O_3 or Cu_2O species cannot be excluded as their quantity present in the sample might be below the XRD detection limit.

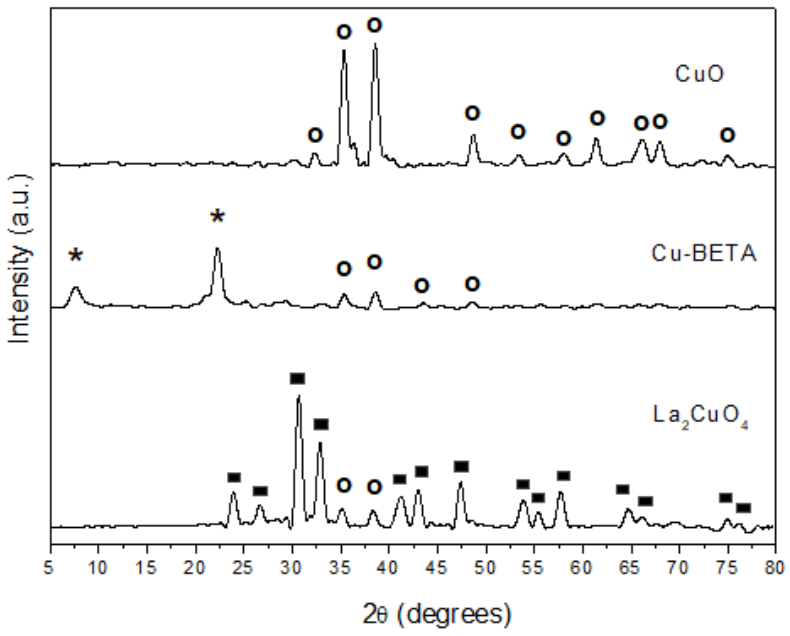

Figure 1 XRD patterns of CuO, Cu-BETA, and La_2CuO_4, in which the symbol (o) indicates the peaks characteristic of copper oxide, (*) BETA zeolite, and (■) La_2CuO_4.

Table 1 shows the average crystallite size of CuO, Cu-BETA, and La_2CuO_4 catalysts. The crystallite size was determined from the XRD data of the samples using the Scherrer equation. The average crystallite size for CuO, La_2CuO_4, and Cu-BETA catalysts is estimated to lie between 15 and 20 nm. Note that Cu-BETA contains a small crystallite size of CuO formed over the large surface area of BETA zeolite (~ 600 m^2/g). This resulted in more Cu^{2+} cations on the surface and exhibited better redox properties. On the other hand, the average crystallite size of CuO and La_2CuO_4 catalysts was 20 nm. It is a known fact that larger CuO particles are reduced at higher temperatures [20]. Therefore, it is interesting to compare the reducibility of these copper-containing catalysts.

Table 1 Chemical composition, crystallite size, and reduction degree of the catalysts.

Catalyst	Copper content [a] (wt. %)	Crystallite size [b] (nm)	Degree of reduction [c] (α)
Cu-BETA	19.70	15	0.99
La_2CuO_4	29.10	20	0.96
CuO	79.43	20	1.00

[a] obtained by X-ray fluorescence (XRF). [b] Average crystallite size calculated by the Debye-Scherrer equation using reflection of CuO (2θ = 38.7°). [c] Relation between mol of H_2 consumed per mol of copper.

H_2-TPR profiles of the CuO, La_2CuO_4, and Cu-BETA catalysts are presented in Figure 2. For all samples, the total hydrogen consumption showed H_2/Cu molar ratio close to one (Table 1), which is in agreement with the theoretical value corresponding to the reduction of Cu^{2+} to Cu^0 (H_2/Cu = 1). The color change from dark blue or black to red-purple after TPR analysis also confirms that complete reduction of Cu^{2+} to Cu° has occurred. Cu-BETA showed peaks at 229 and 356 °C. The peak at 229 °C corresponds to the reduction of dispersed Cu^{2+} to Cu^+ and of CuO nanoparticles (observed by XRD) to Cu^0 [10, 14, 21-23]. The peak at 356 °C can be attributed to the successive reduction of Cu^+ to Cu^0 [21-23]. Thus it can be suggested that Cu-BETA contains both dispersed Cu^{2+} ions and CuO nanoparticles after preparation.

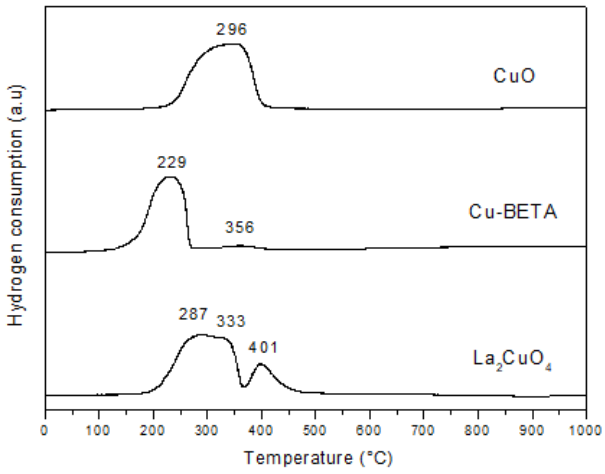

Figure 2 H_2-TPR profiles of the CuO, Cu-BETA, and La_2CuO_4 catalysts.

The data given in Table 1 shows that the copper content of Cu-BETA (19.7 wt.%) exceeds the entire ion exchange capacity of the BETA zeolite (3.9 wt.%), with the assumption that each Cu^{2+} cation needs two ionic exchange sites. Thus, considering the areas under the peaks at 229 °C (A1) and 356 °C (A2) in Figure 2, the distribution of the exchangeable Cu-species (%Cu^{2+} = 2 × (A2/A1+A2) × 19.7) and CuO (%CuO = ((A1-A2)/(A1+A2)) × 19.7) for Cu-BETA (3.0 wt.% of Cu^{2+} and 16.70 wt.% of CuO) can be estimated.

As shown in Figure 2, the reduction of CuO corresponds to a single reduction peak at 296 °C. TPR studies of the reduction of bulk CuO have typically shown a direct transformation to Cu°. The reduction of bulk copper species requires higher temperature in comparison to surface copper species [24]. La_2CuO_4 shows two main reduction peaks: the first peak appears at 287 °C together with a slight shoulder (at 333 °C) assigned to reduction of Cu^{2+} (present in CuO and La_2CuO_4) to Cu^0; another reduction peak at 401 °C is due to the reduction of Cu^+ to Cu^0, which was not reduced in the previous step [25, 26].

Further information on the copper species present in the CuO, La_2CuO_4, and Cu-BETA catalysts was studied by UV-VIS spectroscopy, as shown in Figure 3. Cu-BETA shows absorption bands located at 217 and 255 nm corresponding to charge transfer (CT) transition from the oxygen atoms to exchanged Cu^{2+} in a single site on the zeolite structure [27]. There are also broad absorptions observed in the region of d–d transitions at 400–800 nm corresponding to the octahedral Cu^{2+} in the crystalline structure of CuO [28, 29]. According to the intensity of relative bands, the weak band at about 450 nm characteristic of $(Cu\text{-}O\text{-}Cu)^{2+}$ or di-copper species indicates the prevailing existence of Cu^{2+}, which compensates for the negative charge of the zeolite framework [27, 30, 31]. These results are consistent with the XRD and TPR measurements done on these catalysts. As for the UV–VIS spectra of CuO and La_2CuO_4 catalysts (Figure 3), the shapes of curves are similar to each other, with some minor differences in absorbance. The similarity of the UV–VIS spectra may indicate the presence of the same type of Cu-O bonds and crystallite sizes (see Table 1) among all these catalysts [32]. Figure 3 shows absorption bands located at 330 and 682 nm related to the d-d electronic transitions of copper in CuO and La_2CuO_4 catalysts. A small band at 580 nm can be assigned to Cu^{2+}…Cu^+ intervalence transition (IVT) [28, 33].

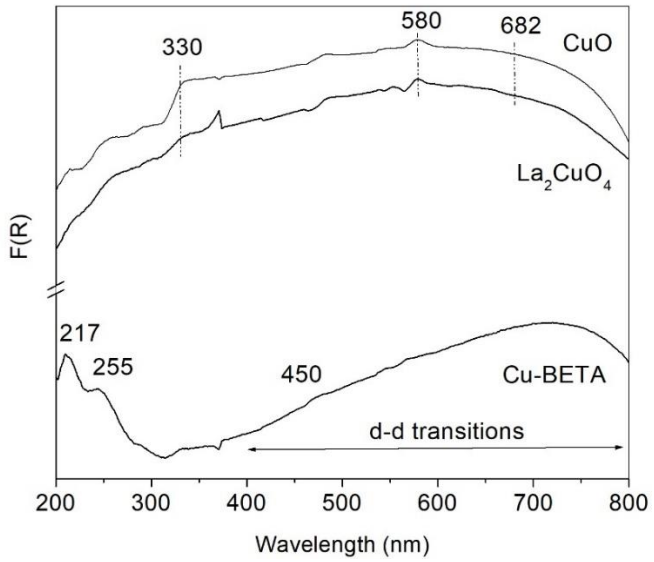

Figure 3 UV-VIS spectra of Cu-BETA, CuO, and La_2CuO_4 catalysts.

In summary, the UV-VIS results show that exchanged and octahedral species of Cu^{2+} coexist in Cu-BETA, while octahedral Cu^{2+} is the predominant species in both CuO and La_2CuO_4 catalysts. Exchanged copper in zeolites has more accentuated CT bands compared to CuO and La_2CuO_4 (Figure 3). These dispersed single Cu^{2+} occupying cationic sites and CuO nanoparticles could also be detected in Cu-zeolites [34].

Figure 4 shows the CH_3CN conversions on Cu-BETA, CuO, and La_2CuO_4 catalysts as a function of reaction temperature. BETA zeolite without copper has practically no activity under the studied conditions (not shown). The copper species are active sites for the CH_3CN-SCC reaction, and the comparison of the catalysts was performed with the same mass of copper introduced into the reactor. It was found that the CH_3CN initial conversion rises rapidly upon increasing the temperature and attains a stable state at a temperature range of 400–600 °C for all catalysts. Cu-BETA has well-dispersed Cu-species, as confirmed by H_2-TPR and UV-VIS analyses, leading to much higher CH_3CN conversion. This attributes to the higher activity of Cu-BETA catalysts than CuO and La_2CuO_4 catalysts, showing that copper species on the zeolite surface are more active due to the lower activation energy barrier for the CH_3CN-SCC reaction. It has been reported that well-dispersed CuO species exhibit much higher oxidation activity and reducibility compared to the exchanged Cu ions [34]. Thus, the Cu-O bonding as it occurs in CuO dispersed over BETA zeolite is the reason for its easy reducibility and high oxidation catalytic activity. As already discussed, the UV-VIS results showed that octahedral Cu^{2+} species are dominant in both CuO and La_2CuO_4 catalysts (Figure 3). However, octahedral Cu^{2+} species in CuO undergo reduction at a lower temperature than La_2CuO_4 (Figure 2). This greater ease of reduction is a favorable factor that can contribute to the improvement of catalytic performances [35-38]. The oxy-reduction properties of the catalysts play a significant role in the CH_3CN-SCC reaction. According to the aforementioned results, the Cu-BETA catalyst had a lower reduction temperature and hence higher CH_3CN conversion rate.

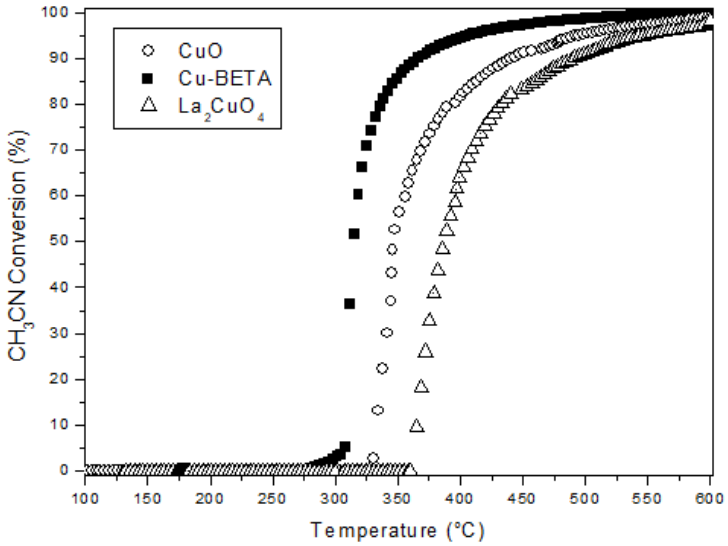

Figure 4 Acetonitrile conversion over Cu-BETA, La_2CuO_4, and CuO catalysts using 2.8 vol.% CH_3CN in airflow (40 mL/min) and 8.6 mg of copper in the sample.

Apart from the high conversion rate of CH_3CN, the high yield of N_2 and CO_2 is another important criterion for choosing the ideal catalyst considering the possibility of releasing other undesirable by-

products (NH_3, N_2O, HCN, NO, and NO_2) during CH_3CN combustion. Figure 5 shows the measure of N-containing products (N_2, NH_3, N_2O, HCN, NO, and NO_2) on Cu-BETA, CuO, and La_2CuO_4 catalysts as a function of reaction temperature. It is worth noting that acetonitrile was oxidized directly to CO_2 by all the catalysts. In addition, CH_3CN was largely transformed into N_2 and other undesirable by-products (N_2O and NO) above 320 °C and 360 °C over CuO and La_2CuO_4 catalysts, respectively. The relatively greater amount of N_2O could be tackled up to 550 °C followed by slightly declining temperatures for CuO (Figure 5a) and La_2CuO_4 (Figure 5b). These undesirable by-products and the lower N_2 yield observed for the CuO and La_2CuO_4 catalysts are very similar to the reported outcome of CuO supported on the SBA-15 catalyst [8]. Therefore, CH_3CN was largely transformed into N_2 and undesirable by-products (N_2O + NO) on octahedral Cu^{2+} species present in CuO and La_2CuO_4 catalysts (Figure 3). On the other hand, Cu-BETA (Figure 5c) showed the highest N_2 yield, which started from 300 °C, increasing progressively with the reaction temperature, and almost remaining stable at a temperature range of 400–600 °C. Thus, the easy reducibility of the highly dispersed Cu-species and the small crystallite size contributed to the better performance of the Cu-BETA catalyst. The discussion suggests that the high conversion of acetonitrile and the highest N_2 yield make Cu-BETA an excellent candidate for catalyzing CH_3CN-SCC.

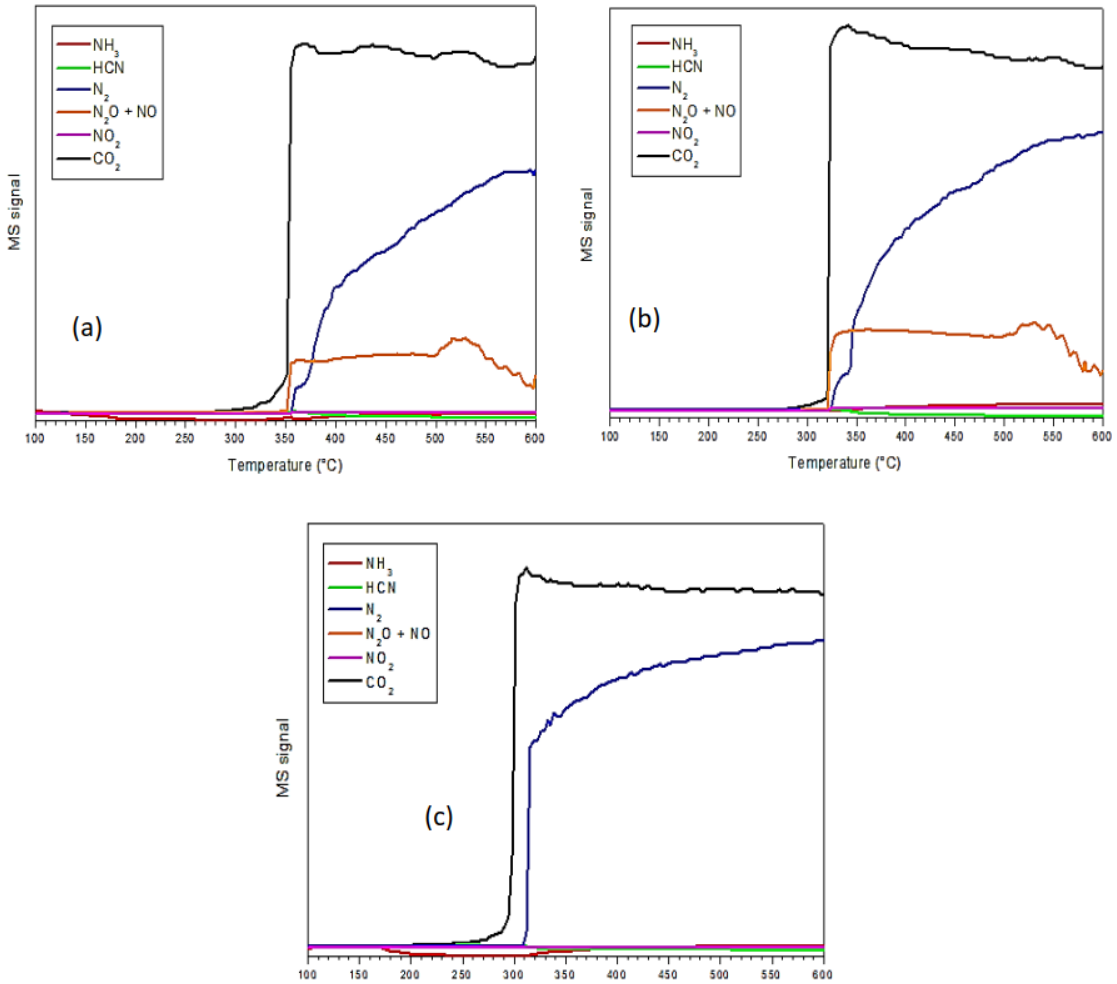

Figure 5 Catalytic performance as a function of temperature during CH_3CN combustion over: (a) CuO; (b) La_2CuO_4; (c) Cu-BETA. Conditions: 2.8% CH_3CN, 20.4% O_2, 8.6 mg of copper in the sample.

Moreover, the stability test of Cu-BETA was performed at 600 °C (Figure 6). It could be seen that Cu-BETA showed a very stable conversion rate (nearly 100%) with a 10 h reaction time (Figure 6a), along with maintaining the desired high yield of N_2 and CO_2 throughout CH_3CN combustion (Figure 6b). Such results affirmed that the Cu-BETA catalyst maintained excellent catalytic activity and N_2 selectivity. Results from the present study could surpass other works reported in the literature [7, 8, 39], where the N_2 selectivity decreases as the reaction proceeds [40]. Cu-BETA also showed exceptionally high turnover frequencies (TOF = 5.3–11.7 × 10^{-4} s^{-1}) at a temperature range of 300–600 °C compared to CuO (TOF = 0.5–2.3 × 10^{-4} s^{-1}) and La_2CuO_4 (TOF = 0–7.8 × 10^{-4} s^{-1}) catalysts. These results show the influence of the catalyst structure on acetonitrile combustion and N_2 selectivity.

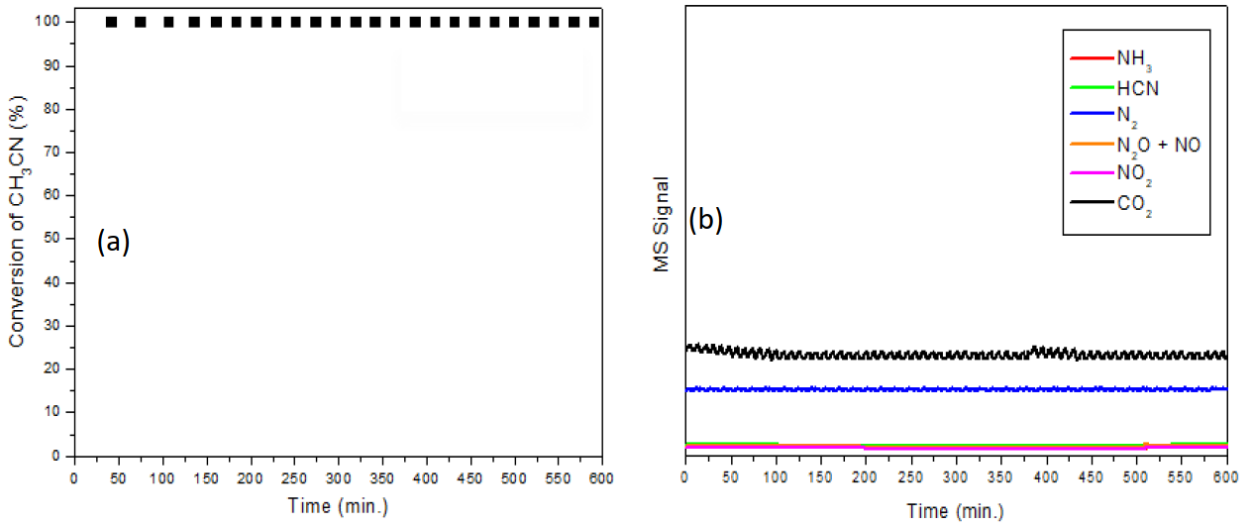

Figure 6 Stability curves of (a) catalytic oxidation of acetonitrile over the Cu-BETA catalyst at 600 °C and (b) measure of products during the reaction.

4. Conclusions

Copper-based nanocatalysts were used for acetonitrile combustion and were subjected to the formation of N-containing products. According to the study, Cu-BETA has both exchanged and octahedral species, while octahedral species are predominant in CuO and La_2CuO_4. CuO, Cu-BETA, and La_2CuO_4 catalysts achieved high conversion rates of acetonitrile, which increased rapidly with temperature. However, CuO and La_2CuO_4 nanocatalysts resulted in the formation of undesired products, N_2O and NO. On the other hand, Cu-BETA nanocatalysts showed excellent activity and high N_2 yield in CH_3CN combustion. The easy reducibility of the highly dispersed Cu-species and its small crystallite size primarily enhance the oxidation activity of acetonitrile as well as N_2 yield. Furthermore, Cu-BETA has shown exceptional stability. Therefore, the high conversion rate of acetonitrile and the high N_2 selectivity make Cu-BETA a potent candidate for C_3CN-SCC.

Acknowledgments

We are grateful to the Prof. Luiz Carlos A. Oliveira for collaboration with UV-VIS spectroscopy analysis.

Author Contributions

Mrs. Jéssica A. P. Ponciano performed experiments and analyses. Prof. Marcelo S. Batista supervised the research.

Funding

We are grateful to the FAPEMIG for the scholarships.

Competing Interests

The authors have declared that no competing interests exist.

References

1. Johnson LD, Fuerst RG, Steger JL, Bursey JT. Evaluation of a sampling method for acetonitrile emissions from stationary sources. Proceedings of the EPA/A&WMA International Symposium: Measurement of Toxic and Related Air Pollutants; 1997 April; NC, USA. Washington: United States Environmental Protection Agency. pp.149-158.
2. Nasr FA, Mikhaeil B. Treatment of domestic wastewater using conventional and baffled septic tanks. Environ Technol. 2013; 34: 2337-2343.
3. Liu N, Shi D, Zhang R, Li Y, Chen B. Highly selective catalytic combustion of acrylonitrile towards nitrogen over Cu-modified zeolites. Catal Today. 2019; 332: 201-213.
4. Alzueta MU, Guerrero M, Millera Á, Marshall P, Glarborg P. Experimental and kinetic modeling study of oxidation of acetonitrile. Proc Combust Inst. 2021; 38: 575-583.
5. Zhang R, Liu N, Lei Z, Chen B. Selective transformation of various nitrogen-containing exhaust gases toward N_2 over zeolite catalysts. Chem Rev. 2016; 116: 3658-3721.
6. Dong F, Han W, Zhao H, Zhang G, Tang Z. Porous hollow CoInOx nanocubes as a highly efficient catalyst for the catalytic combustion of toluene. Nanoscale. 2019; 11: 9937-9948.
7. Wang Y, Ying Q, Zhang Y, Liu Y, Wu Z. Reaction behaviors of CH_3CN catalytic combustion over $CuCeO_x$-HZSM-5 composite catalysts: The mechanism of enhanced N_2 selectivity. Appl Catal A Gen. 2020; 590: 117373.
8. Zhang R, Shi D, Liu N, Cao Y, Chen B. Mesoporous SBA-15 promoted by 3d-transition and noble metals for catalytic combustion of acetonitrile. Appl Catal B. 2014; 146: 79-93.
9. Zhang R, Shi D, Liu N, Chen B, Wu L, Wu L, et al. Catalytic purification of acrylonitrile-containing exhaust gases from petrochemical industry by metal-doped mesoporous zeolites. Catal Today. 2015; 258: 17-27.
10. Nanba T, Masukawa S, Uchisawa J, Obuchi A. Screening of catalysts for acrylonitrile decomposition. Catal Letters. 2004; 93: 195-201.
11. Granger P, Parvulescu VI, Kaliaguine S, Prellier W. Perovskites and related mixed oxides: Concepts and applications. Weinheim: John Wiley & Sons; 2015.
12. Zhang R, Li P, Xiao R, Liu N, Chen B. Insight into the mechanism of catalytic combustion of acrylonitrile over Cu-doped perovskites by an experimental and theoretical study. Appl Catal B. 2016; 196: 142-154.

13. Nanba T, Masukawa S, Uchisawa J, Obuchi A. Mechanism of acrylonitrile decomposition over Cu-ZSM-5. J Mol Catal A Chem. 2007; 276: 130-136.
14. Nanba T, Masukawa S, Ogata A, Uchisawa J, Obuchi A. Active sites of Cu-ZSM-5 for the decomposition of acrylonitrile. Appl Catal B. 2005; 61: 288-296.
15. Øygarden AH, Pérez-Ramírez J. Activity of commercial zeolites with iron impurities in direct N_2O decomposition. Appl Catal B. 2006; 65: 163-167.
16. Chen B, Liu N, Liu X, Zhang R, Li Y, Li Y, et al. Study on the direct decomposition of nitrous oxide over Fe-beta zeolites: From experiment to theory. Catal Today. 2011; 175: 245-255.
17. Liu N, Yuan X, Zhang R, Li Y, Chen B. Mechanistic insight into selective catalytic combustion of HCN over Cu-BEA: Influence of different active center structures. Phys Chem Chem Phys. 2017; 19: 23960-23970.
18. Dharmadhikari DV, Nikam SK, Athawale AA. Template free hydrothermal synthesis and gas sensing application of lanthanum cuprate (La_2CuO_4): Effect of precursors on phase formation and morphology. J Alloys Compd. 2014; 590: 486-493.
19. Cavalheiro AA, Zaghete MA, Santos CO, Varela JA, Longo E. Influence of synthesis and processing parameters of the columbite precursor on the amount of Perovskite PMN. Mat Res. 1999; 2: 255-260.
20. Kundakovic L, Flytzani-Stephanopoulos M. Reduction characteristics of copper oxide in cerium and zirconium oxide systems. Appl Catal A Gen. 1998; 171: 13-29.
21. Vennestrøm PN, Janssens TV, Kustov A, Grill M, Puig-Molina A, Lundegaard LF, et al. Influence of lattice stability on hydrothermal deactivation of Cu-ZSM-5 and Cu-IM-5 zeolites for selective catalytic reduction of NO_x by NH_3. J Catal. 2014; 309: 477-490.
22. Urquieta-González EA, Martins L, Peguin RP, Batista MS. Identification of extra-framework species on Fe/ZSM-5 and Cu/ZSM-5 catalysts typical microporous molecular sieves with zeolitic structure. Mat Res. 2002; 5: 321-327.
23. Lai S, Meng D, Zhan W, Guo Y, Guo Y, Zhang Z, et al. The promotional role of Ce in Cu/ZSM-5 and in situ surface reaction for selective catalytic reduction of NO_x with NH_3. RSC Adv. 2015; 5: 90235-90244.
24. Śliwa M, Samson K. Influence of synthesis parameters on physicochemical properties of CuO/ZrO_2 catalysts. Chem Zvesti. 2019; 73: 2793-2802.
25. Thao NT. Synthesis of Co-Cu/La_2O_3 Pervoskites for Hydrogenation of CO. Asian J Chem. 2013; 25: 8082-8086.
26. Velasquez M, Santamaria A, Batiot-Dupeyrat C. Selective conversion of glycerol to hydroxyacetone in gas phase over La_2CuO_4 catalyst. Appl Catal B. 2014; 160: 606-613.
27. Sazama P, Pilar R, Mokrzycki L, Vondrova A, Kaucky D, Plsek J, et al. Remarkably enhanced density and specific activity of active sites in Al-rich Cu-, Fe-and Co-beta zeolites for selective catalytic reduction of NO_x. Appl Catal B. 2016; 189: 65-74.
28. Ismagilov ZR, Yashnik SA, Anufrienko VF, Larina TV, Vasenin NT, Bulgakov NN, et al. Linear nanoscale clusters of CuO in Cu-ZSM-5 catalysts. Appl Surf Sci. 2004; 226: 88-93.
29. Zhang Y, Chen C, Lin X, Li D, Chen X, Zhan Y, et al. CuO/ZrO_2 catalysts for water-gas shift reaction: Nature of catalytically active copper species. Int J Hydrog Energy. 2014; 39: 3746-3754.
30. Xu L, Shi C, Chen B, Zhao Q, Zhu Y, Gies H, et al. Improvement of catalytic activity over Cu--Fe modified Al-rich Beta catalyst for the selective catalytic reduction of NO_x with NH_3. Microporous Mesoporous Mater. 2016; 236: 211-217.

31. Giordanino F, Vennestrøm PN, Lundegaard LF, Stappen FN, Mossin S, Beato P, et al. Characterization of Cu-exchanged SSZ-13: A comparative FTIR, UV-Vis, and EPR study with Cu-ZSM-5 and Cu-β with similar Si/Al and Cu/Al ratios. Dalton Trans. 2013; 42: 12741-12761.
32. Yin M, Wu CK, Lou Y, Burda C, Koberstein JT, Zhu Y, et al. Copper oxide nanocrystals. J Am Chem Soc. 2005; 127: 9506-9511.
33. Stiedl J, Green S, Chassé T, Rebner K. Auger electron spectroscopy and UV–Vis spectroscopy in combination with multivariate curve resolution analysis to determine the Cu_2O/CuO ratios in oxide layers on technical copper surfaces. Appl Surf Sci. 2019; 486: 354-361.
34. Bulánek R, Wichterlová B, Sobalık Z, Tichý J. Reducibility and oxidation activity of Cu ions in zeolites: Effect of Cu ion coordination and zeolite framework composition. Appl Catal B. 2001; 31: 13-25.
35. Castaño MH, Molina R, Moreno S. Catalytic oxidation of VOCs on $MnMgAlO_x$ mixed oxides obtained by auto-combustion. J Mol Catal A Chem. 2015; 398: 358-367.
36. Caldas PC, Gallo JM, Lopez-Castillo A, Zanchet D, Bueno JM. The structure of the Cu-CuO sites determines the catalytic activity of Cu nanoparticles. ACS Catal. 2017; 7: 2419-2424.
37. Wang F, Buchel R, Savitsky A, Zalibera M, Widmann D, Pratsinis SE, et al. In situ EPR study of the redox properties of CuO-CeO_2 catalysts for preferential CO oxidation (PROX). ACS Catal. 2016; 6: 3520-3530.
38. Papavasiliou J, Rawski M, Vakros J, Avgouropoulos G. A novel post-synthesis modification of CuO-CeO_2 catalysts: Effect on their activity for selective CO oxidation. ChemCatChem 2018; 10: 2096-2106.
39. Karakas G, Sevinc A. Catalytic oxidation of nitrogen containing compounds for nitrogen determination. Catal Today. 2019; 323: 159-165.
40. Zhang Y, Wang Y, Liu Y, Ying Q, Wu Z. Catalytic combustion of acetonitrile over $CuCeO_x$-HZSM-5 composite catalysts with different mass ratios: The synergism between oxidation and hydrolysis reactions. J Colloid Interface Sci. 2021; 584: 193-203.